

# Automation Assisted Anaerobic Phenotyping For Metabolic Engineering

Kaushik Raj<sup>1,\*</sup>, Naveen Venayak<sup>1,\*</sup>, Patrick Diep<sup>1</sup>, Sai Akhil Golla<sup>1</sup>, Alexander F. Yakunin<sup>1,2</sup>,  
and Radhakrishnan Mahadevan<sup>1,3,\*\*</sup>

<sup>1</sup>Department of Chemical Engineering and Applied Chemistry, University of Toronto, Canada

<sup>2</sup>Centre for Environmental Biotechnology, School of Natural Sciences, Bangor University, U.K.

<sup>3</sup>Institute of Biomaterials and Biomedical Engineering, University of Toronto, Canada

\*These authors contributed equally

\*\*Corresponding author. Address: 200 College Street, Toronto, Ontario - M5G 2J8, Canada.

Email: [krishna.mahadevan@utoronto.ca](mailto:krishna.mahadevan@utoronto.ca)

## Abstract

Microorganisms can be metabolically engineered to produce a wide range of commercially important chemicals. Advancements in computational strategies for strain design and synthetic biological techniques to construct the designed strains have facilitated the generation of large libraries of potential candidates for chemical production. Consequently, there is a need for a high-throughput, laboratory scale techniques to characterize and screen these candidates to select strains for further investigation in large scale fermentation processes. Several small-scale fermentation techniques, in conjunction with laboratory automation have enhanced the throughput of enzyme and strain phenotyping experiments. However, such high throughput experimentation typically entails large operational costs and generate massive amounts of laboratory plastic waste. In this work, we develop an eco-friendly automation workflow that effectively calibrates and decontaminates fixed-tip liquid handling systems to reduce tip waste. We also investigate inexpensive methods to establish anaerobic conditions in microplates for high-throughput anaerobic phenotyping. To validate our phenotyping platform, we perform two case studies - an anaerobic enzyme screen, and a microbial phenotypic screen. We used our automation platform to investigate conditions under which several strains of *E. coli* exhibit the same phenotypes in 0.5 L bioreactors and in our scaled-down fermentation platform. Further, we propose the use of dimensionality reduction through t-distributed stochastic neighbours embedding in conjunction with our phenotyping platform to serve as an effective scale-down model for bioreactor phenotypes. By integrating an in-house data-analysis pipeline, we were able to accelerate the 'test' phase of the design-build-test-learn cycle of metabolic engineering.

## Introduction

Microbial production of chemicals has gained prominence in the past few decades due to rising populations and increased concerns over the sustainability of conventional means of chemical production.

24 Advances in metabolic engineering and synthetic biology have enabled the generation of mutant strains  
25 that are adept at producing a wide range of natural and non-natural chemicals<sup>32</sup>. However, a myriad of  
26 scale-up issues can arise at increasingly larger scales, that could render many microbial production plat-  
27 forms economically infeasible<sup>8,24</sup>. Hence, several iterations of the design-build-test-learn (DBTL) cycle  
28 (Figure 1a) may be required at smaller scales before moving on to production in larger scale bioreactors.

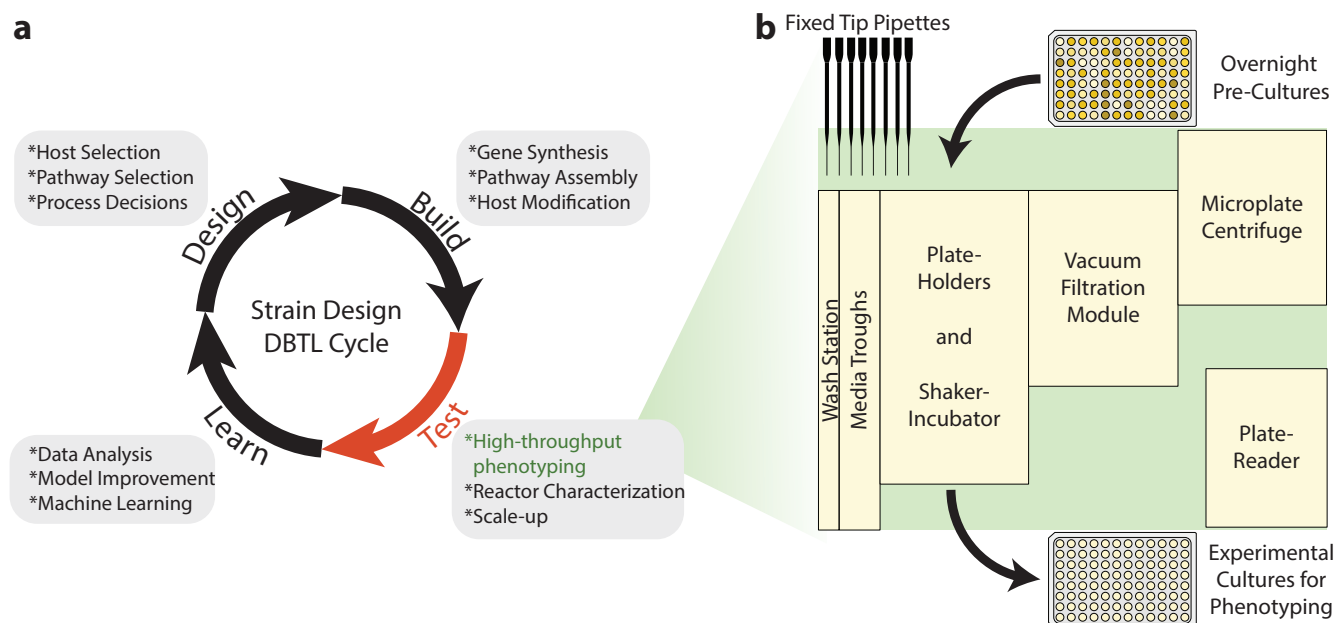


**Figure 1: DBTL cycle in metabolic engineering and layout of phenotyping platform a.** Typical decisions and tasks involved in each step of the DBTL cycle for strain engineering. Test cycle remains a bottleneck due to the time and costs incurred in phenotyping a large number of strains/enzymes. **b.** Deck layout of liquid handling platform used in this study. Relatively few equipment can be assembled and repurposed to establish an effective high-throughput phenotyping platform.

29 The development of genome-scale metabolic models and computational tools that use these models to  
30 predict genetic interventions for strain design has assisted the 'design' phase of the DBTL cycle<sup>4,11,43,52</sup>.  
31 Similarly, advances in DNA synthesis, computational tools to streamline DNA assembly, and the establish-  
32 ment of DNA foundries around the world have also allowed for the rapid construction of mutant strain and  
33 enzyme libraries that incorporate these intervention strategies, accelerating the 'build' phase<sup>5,16,18,27,37</sup>.  
34 The 'test' phase i.e. characterization/phenotyping of the strain and enzyme libraries generated in the  
35 'design' and 'build' phases of the DBTL cycle remains a key bottleneck. The prohibitive cost of analyzing  
36 the phenotypes of all microbial strains in the generated mutant libraries using laboratory scale bioreac-  
37 tors necessitates the development of standardized high-throughput, small-scale protocols to characterize  
38 them. Recently, several machine learning techniques have been adapted for metabolic engineering ap-  
39 plications, with several tools being developed that promise to assist the 'learn' phase<sup>31,41</sup>. These tools  
40 also necessitate the generation of large and reliable experimental phenotypic datasets that are only eco-  
41 nomically feasible at extremely small scales, further bolstering the need for protocols for high-throughput  
42 phenotyping platforms<sup>6</sup>.

43 In the recent past, there have been several attempts to develop small scale fermentation platforms  
44 using miniature bioreactors and specialized microplates to cultivate and characterize strains, increasing

45 experimental throughput<sup>2,25,29</sup>. However, the operational costs of using such systems is quite high due to  
46 the requirement of specialized microplates and intricate pH control mechanisms. Further, the automation  
47 of strain cultivation and other routine workflows to enhance throughput using such systems may be very  
48 expensive to implement. The earliest attempts at high-throughput fermentation were through the use  
49 of standard 96-well microtiter plates for parallel cultivation of microbes.<sup>10</sup> The low cost and enhanced  
50 throughput of these systems made them very valuable to perform preliminary screens on a large number  
51 of strains. However, these systems suffer from several disadvantages including increased rates of sample  
52 evaporation and reduced oxygen transfer. Therefore, microbial phenotypes observed in these scales may  
53 not be replicable at the scale of bench-top reactors under aerobic conditions. Yet, these systems may  
54 still be suitable to phenotype microbes under anaerobic conditions where oxygen transfer is not crucial.  
55 *E. coli* can be engineered to produce an array of commercially important compounds such as lactic acid  
56 under anaerobic conditions<sup>9,35</sup>. Moreover, the production phase of many industrial fermentation processes  
57 involve high density cultures where oxygen transfer is limited. Microtiter plates are particularly suited  
58 for anaerobic fermentations due to the inherent difficulty in achieving high oxygen transfer rates and have  
59 the potential to be able to replicate the phenotypes of microbes observed in bench-top bioreactors.

60 The advent of liquid handling systems has assisted in the use of such small-scale fermentation plat-  
61 forms, enhancing throughput by reducing human effort and time required to set up phenotyping experi-  
62 ments<sup>7,17,44,47</sup>. Use of such automation systems also enhances the reproducibility of experiments through  
63 the use of standardized protocols. While automated liquid handling platforms can rapidly accelerate  
64 the throughput of experiments, maintaining sterile conditions during long high throughput workflows is  
65 challenging. Contamination arising from the environment can be effectively curbed through the use of  
66 HEPA filters<sup>20</sup>. However, cross-contamination resulting from tip carryover could still be a problem, since  
67 any residual contaminant in the components of the platform could potentially confound results from a  
68 large set of experiments. Liquid handling systems with disposable tips have been successfully adapted to  
69 cultivate cells and perform other routine microbiological workflows with minimal contamination<sup>20,26,46</sup>.  
70 These systems simply discard used and contaminated tips after each pipetting step, thereby eliminating  
71 contamination. This would inevitably result in massive amounts of plastic waste when such systems are  
72 used for high-throughput workflows. The rapidly increasing adoption of automated workflows in research  
73 laboratories would only exacerbate this problem due to their increased throughput<sup>19</sup>. Moreover, the  
74 need for a massive number of sterilized tips would increase the operational costs required to implement  
75 such workflows<sup>28,46</sup>. The use of fixed-tip liquid handlers with effective decontamination protocols could  
76 address concerns about sustainability and operational costs.

77 In this work, we describe several efforts towards enhancing the utility of fixed-tip liquid handling sys-  
78 tems for automated high-throughput phenotyping using a platform consisting of a fixed-tip liquid handler,  
79 microplate centrifuge, plate-reader, vacuum filtration module, plate handling robot, and a shaker incu-  
80 bator (Figure 1b). To this end, we develop decontamination protocols to eliminate microbial carry-over  
81 and cross-contamination in fixed-tip liquid handlers, describe an automated calibration workflow to cal-  
82 ibrate liquid handling pipettes, and establish relatively easy methods to ensure anaerobicity of media  
83 for anaerobic phenotyping. Then, we validate our platform by performing an anaerobic enzyme screen  
84 and investigate conditions that allow reasonable replication of bioreactor microbial phenotypes in 96-well  
85 microplates.

86

87

## 88 Results & Discussion

### 89 A decontamination protocol for fixed-tip liquid handlers

90 Fixed-tip liquid handling systems require decontamination after every pipetting step to curb biological  
91 cross-contamination. A disinfection step where tips are washed and incubated with ethanol has been  
92 proposed in the past to address contamination issues<sup>44</sup>. However, this protocol required the incubation  
93 of pipette tips in ethanol for five minutes between each pipetting step, reducing the throughput of  
94 this system. More recently, one study used a layer of ethanol, aspirated immediately before aspirating  
95 biological samples to maintain sterility.<sup>23</sup>. While this protocol is faster, it may result in reduced cell  
viability due to direct contact between the disinfectant and cells.

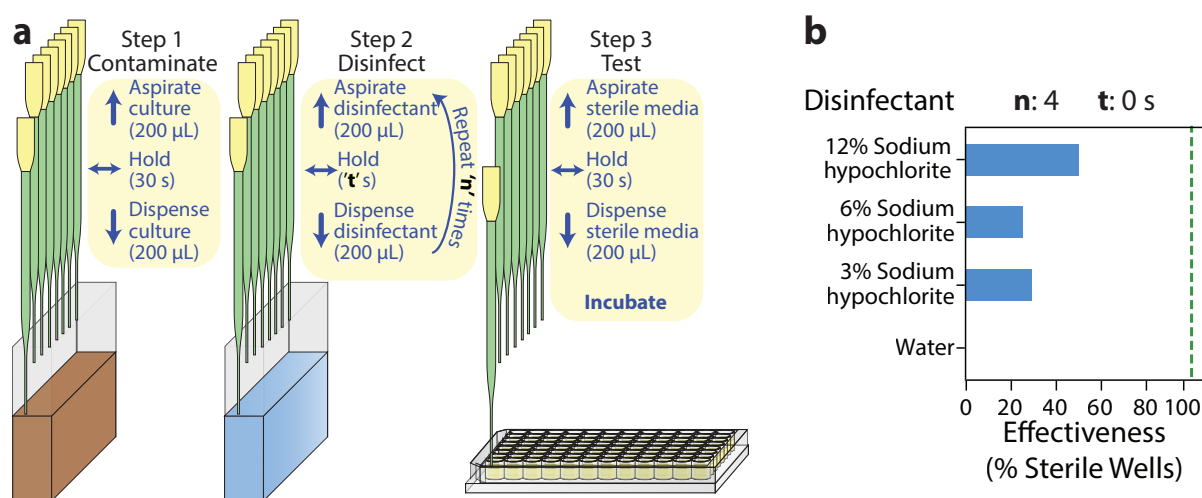


**Figure 2: Preliminary decontamination protocol a.** Steps to decontaminate and investigate effectiveness of the decontamination protocol. ' $n$ ' represents the number of washes with the disinfectant and ' $t$ ' represents the duration for which the disinfectant is held within the tips for each wash. **b.** Initial decontamination test using different concentrations of sodium hypochlorite(bleach) with ' $n$ '=4 and ' $t$ '=0 and the default air-gap of the system (10 µL). Each bar represents effectiveness calculated from 24 replicates.

96

97 To address these issues, we examined the effectiveness of a simple decontamination protocol that uses  
98 a solution of sodium hypochlorite (bleach) to disinfect pipette tips (Figure 2a). In order to simulate  
99 typical contamination events during cell culture workflows, we programmed the pipette to aspirate 200  
100 µL of viable *E. coli* cells in their exponential phase of growth, hold for 30 seconds with the pipette  
101 tips dipped inside the culture, and dispense the cells back into the solution. Then, the tips aspirate 400  
102 µL of bleach, hold for a specified interval - ' $t$ ' seconds with the tips dipped inside, and dispense the  
103 disinfectant. We repeat this bleach wash for a specified number of times - ' $n$ ' and when complete, wash  
104 the tips with system liquid - sterilized ultrapure water, to remove any traces of the disinfectant. Finally,  
105 to examine the effectiveness of our decontamination procedure, we aspirate 200 µL of sterile LB media  
106 from a microplate, hold for 30 seconds and dispense back into the same wells. Any persisting *E. coli* cells

107 in the tips would lead to contamination of the media and show cell growth after incubation of the plate.  
108 We used a wash with water as a negative decontamination control to ensure that contamination events  
109 are captured effectively using this procedure.

110 First, we examined the efficacy of this procedure using varying concentrations of bleach, with ' $n$ '=4  
111 washes and zero hold time (' $t$ ' = 0 s). The sterilization effectiveness was calculated as the percentage of  
112 contaminated wells resulting from the corresponding decontamination procedure. As seen in Figure 2b,  
113 the negative control - water resulted in zero effectiveness. Increasing the concentration of bleach seemed  
114 to positively impact the effectiveness of our protocol. However, even at the highest concentration of  
115 bleach, we only observed a 50% effectiveness of decontamination. We considered that varying the number  
116 of washes - ' $n$ ' and the hold time for the disinfectant - ' $t$ ' could improve our system due to longer  
117 contact with bleach. Increasing the number of washes and the hold time indeed had a positive impact  
118 on the sterilization effectiveness, with the best values being achieved at the highest levels of ' $n$ ' and  
119 ' $t$ ' (Figure 2d - top-left panel). However, this was still unacceptable as the target was to completely  
120 eliminate contamination events. Moreover, operating at the highest levels of ' $n$ ' and ' $t$ ' increased the  
121 run-time of the decontamination protocol to about 1 minute and would therefore reduce the throughput  
122 of our system.

123 Upon further investigation of the pipetting protocol, we observed that like most fixed-tip liquid  
124 handling systems, our pipettes aspirate a very small amount of air (10  $\mu$ L) before each pipetting step to  
125 separate the system liquid from the liquid being pipetted - the process liquid(Figure 3a). By increasing  
126 this air-gap, we were able to remarkably improve our decontamination protocol, achieving complete  
127 sterilization using an air-gap of 250  $\mu$ L (Figure 3b and Supplementary Figure S1). Interestingly, at  
128 the highest level of air-gap, we observed zero contamination events even at our lowest levels of ' $n$ ' and  
129 ' $t$ '. It appears that when the volume of the air-gap is less than the maximum operating volume of the  
130 process liquid, there is a possibility for the sterile system liquid to come in direct contact with parts  
131 of the pipette that have not yet been disinfected. The system liquid is therefore compromised and  
132 could harbour viable cells, which increases the possibility of contamination during further pipetting steps  
133 (Figure 3c). An air-gap greater than the highest process volume ensures complete separation of the  
134 system and process liquids, leading to proper decontamination(Figure 3c). We found that our protocol  
135 remained effective over a range of bleach concentrations and with 70% ethanol even at the lowest levels  
136 of ' $n$ ' and ' $t$ '(Figure 3d). For all further experiments, we chose to use two washes with 6% bleach as the  
137 disinfectant. The duration of the entire decontamination procedure is about 10 seconds and is therefore  
138 at par with the throughput achieved using disposable plastic tips, with no plastic waste generated and  
139 minimal amounts of disinfectant used.

## 140 **Automated photometric calibration of liquid handling pipettes**

141 Following the implementation of our decontamination protocol, we observed that the accuracy of the  
142 pipettes had diminished quite significantly, with aberrant volumes being pipetted consistently. In order  
143 to examine the pipetting accuracy of the liquid handler before and after changing the air-gap, we used  
144 a photometric assay to compare the volumes pipetted by the automated platform to manually pipetted  
145 standards, similar to an assay described previously<sup>45</sup>. In our assay, we used an aqueous solution of  
146 potassium dichromate ( $K_2Cr_2O_7$ ) within concentration ranges that showed a linear relationship with

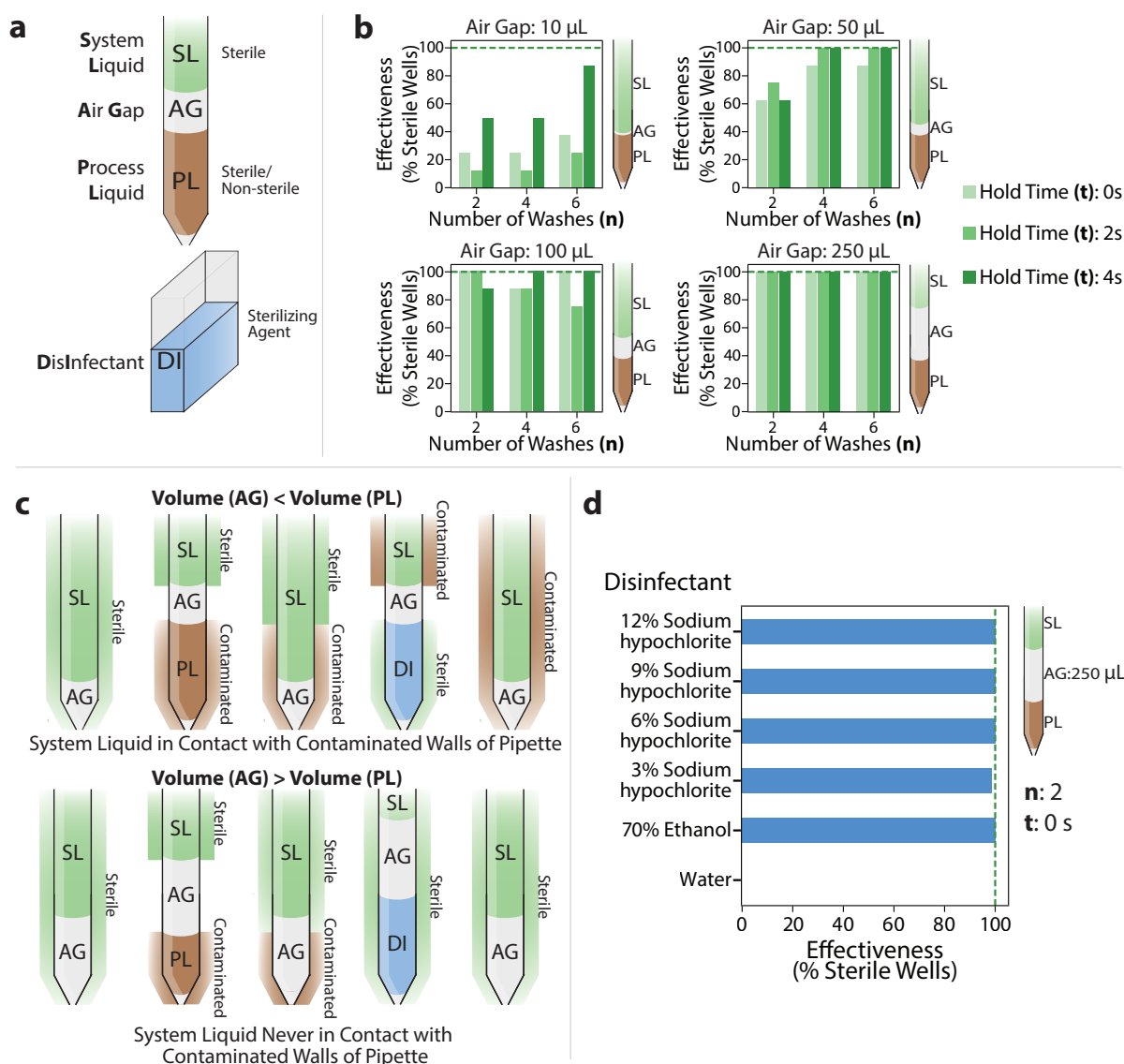


**Figure 3: Optimizing decontamination protocol** **a.** Schematic showing tip layout during a typical pipetting step. **b.** Effect of varying the air-gap on the effectiveness of sterilization using 12% sodium hypochlorite for different values of 'n' - number of disinfectant washes and 't' - disinfectant hold time. Each bar represents effectiveness calculated from 8 replicates. Negative controls using water as the disinfectant resulted in zero sterilization effectiveness for all values of 'n' and 't'. **c.** Proposed mechanism for enhanced sterility upon increasing the volume of the air-gap to be larger than pipetted volumes. **d.** Sterilization effectiveness for different disinfectants with an air-gap of 250  $\mu\text{L}$ . Each bar represents effectiveness calculated from 72 replicates.

147 absorbance at 350 nm, as a photometric standard. We pipetted different levels of the standard within  
 148 volume ranges required during routine operation (3  $\mu\text{L}$  - 200  $\mu\text{L}$ ) into a microplate. Then, an on-deck  
 149 plate reader was used to measure the absorbance and determine the concentration of samples in each  
 150 well, thereby providing an accurate estimate of the pipetted volumes. We observed that after increasing  
 151 the air-gap, the pipetting error increased significantly for all pipette tips (Figure 4a), with values of up  
 152 to 40% for some tips, implying that pipetting accuracy would depend on the volume of air-gap used for  
 153 each pipetting step. The deviations in pipetted volumes were well above the maximum acceptable limits

154 specified by the International Organization for Standardization<sup>22</sup> and would certainly hinder normal  
 155 operation of the platform.

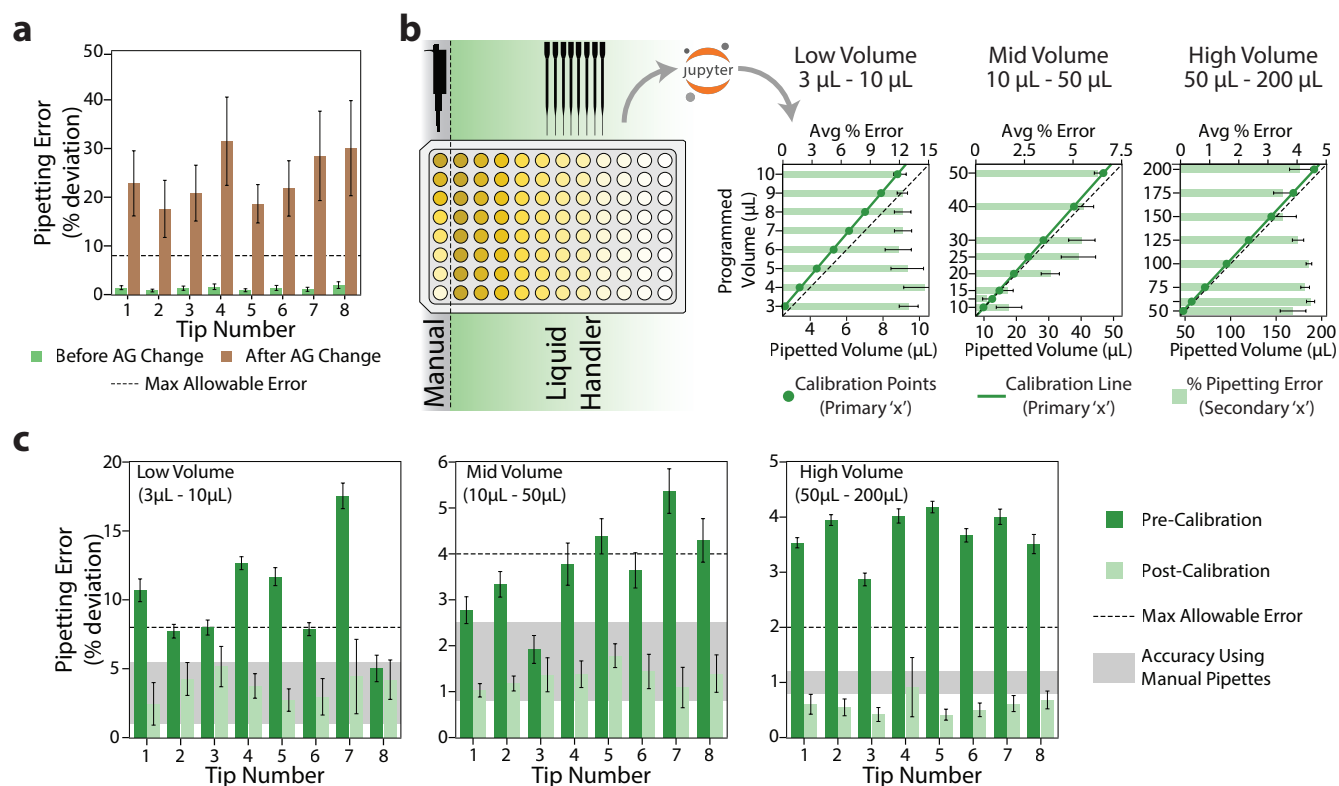


**Figure 4: Automated Photometric Pipette Calibration** **a.** Change in pipetting error due to an increase in the air gap. **b.** Workflow for automated photometric calibration. The liquid handler is made to pipette a photometric standard at different levels onto a microplate. The absorbance data of the microplate are recorded and fed to a pythonic script which automatically calculates pipetting errors and calibration parameters for the pipette. **c.** Pre and post-calibration pipetting error with the air-gap adjusted to ensure sterility. The maximum allowable error was obtained from ISO8655 standards. Accuracy ranges for manual pipettes were obtained from various manufacturers of multi-channel pipettes.

156 Anticipating that there would be a need to vary the pipetting air-gap in the future to accomodate  
 157 different operating volumes, we wished to develop a procedure that would enable quick and reliable  
 158 determination of calibration parameters for the pipette tips. While automated gravimetric methods have  
 159 been explored in the past for calibrating liquid handling pipettes, these would require the presence of  
 160 a specialized, on-deck high-accuracy balance with minimal air-flow to prevent evaporation<sup>1</sup>, which may  
 161 not be available on most liquid handling decks. We expected that the volume estimates calculated using  
 162 the photometric standard could be used to calibrate the pipettes. Upon analysis, we found a strong linear  
 163 correlation between the pipetted volumes and the expected volumes within three different volume ranges  
 164 - high (50 µL - 200 µL), mid (10 µL - 50 µL), and low (3 µL - 10 µL). Hence, we programmed the liquid  
 165 handler to pipette eight different levels of the photometric standard within the three volume ranges in  
 166 triplicate (Figure 4b). To enable automated processing of the data, we developed a python based script  
 167 that accepts the absorbance data of the photometric standard along with the layout of the microplate  
 168 used for calibration to determine the pipetting error for each volume pipetted. The script is then made  
 169 to generate calibration parameters by performing a linear fit between the programmed/ expected volume

170 and the actual pipetted volume. Using these parameters it is possible to determine the volume that  
171 needs to be programmed into the liquid handler for a required volume to be pipetted. Using these new  
172 calibration parameters, we analyzed the pipetting accuracy for each of the custom volume ranges with  
173 the increased air-gap. We found that our photometric calibration procedure reduced the deviation for  
174 all pipette tips significantly and brought them well below the maximum acceptable limits and within  
175 the ranges guaranteed by pipette manufacturers for multi-channel pipettes (Figure 4c). By using only  
176 on-deck components for calibration and a python script to automatically calculate calibration parameters,  
177 we were able to reduce the time required for calibrating each volume range to about 10 minutes. This  
178 protocol and the python script can be easily adapted to calibrate a wide variety of liquid handlers and  
179 conserve accuracy when changing the pipetting parameters.

## 180 **Maintaining sustained anaerobic environments in microplates**

181 Having established protocols to eliminate contamination and calibrate pipettes, we aimed to investigate  
182 our platform's ability to accelerate the 'test' phase of the DBTL cycle in metabolic engineering. As  
183 mentioned before, we were particularly interested in developing protocols for anaerobic phenotyping of  
184 enzymes and microbial strains in microplates due to the oxygen limiting nature of most high density  
185 fermentation processes. Short enzyme assays under anaerobic conditions can be achieved with relative  
186 ease through the addition of the oxygen scavenging enzymes such as glucose oxidase or Oxyrase along with  
187 suitable substrates<sup>12</sup> in each well of the microplate. However, accurate phenotyping of microbial strains  
188 under anaerobic conditions using such enzymatic de-oxygenation would be challenging due to the need  
189 for glucose or other substrates for the enzymes to function. This would hinder accurate quantification  
190 of these metabolites after fermentation, resulting in incomplete carbon balances. Therefore, we decided  
191 to use an anaerobic chamber to remove oxygen from the microplate by subjecting it through cycles of  
192 vacuum and flushing with nitrogen gas.

193 While anaerobic chambers are excellent for expelling oxygen from microplates, they require additional  
194 sophisticated equipment to control humidity. Without humidity control, the evaporation rates within  
195 anaerobic chambers are quite high, resulting in loss of media volume. Upon culturing different *E. coli*  
196 strains within the anaerobic chamber, we found that the rates of evaporation were so high that accurate  
197 measurements of cell density could not be made even though the duration of our fermentations were quite  
198 short (Supplementary Figure S3). As a possible solution, we examined the sealing efficacy of various  
199 adhesive films to sustain the anoxic conditions generated within the anaerobic chamber for fermentations  
200 outside. To measure of oxygen penetration into the microplate, we calculated biomass yields (ratio of  
201 final to initial biomass, measured as absorbance at 600 nm) of wild type *E. coli* (MG1655) grown to  
202 saturation in a rich defined medium within each well. Since *E. coli* grows faster under aerobic conditions,  
203 we should expect a consequent higher yield in wells that have increased oxygen penetration and low yields  
204 where anoxic conditions were sustained. As expected, in our control with a gas permeable film, we found  
205 a relatively high median biomass yield - characteristic of high oxygen penetration (Figure 5a). The use  
206 of a microplate lid with anaerobic adhesive tape did not offer much improvement in the seal, with only a  
207 modest decrease in the median biomass yield. The aluminium and polyester seals (typically used in PCRs)  
208 offered a significant improvement in the seal, with the polyester film being able to reduce the variability  
209 amongst wells as well. However, upon analysis of the biomass yield distribution within the microplates,



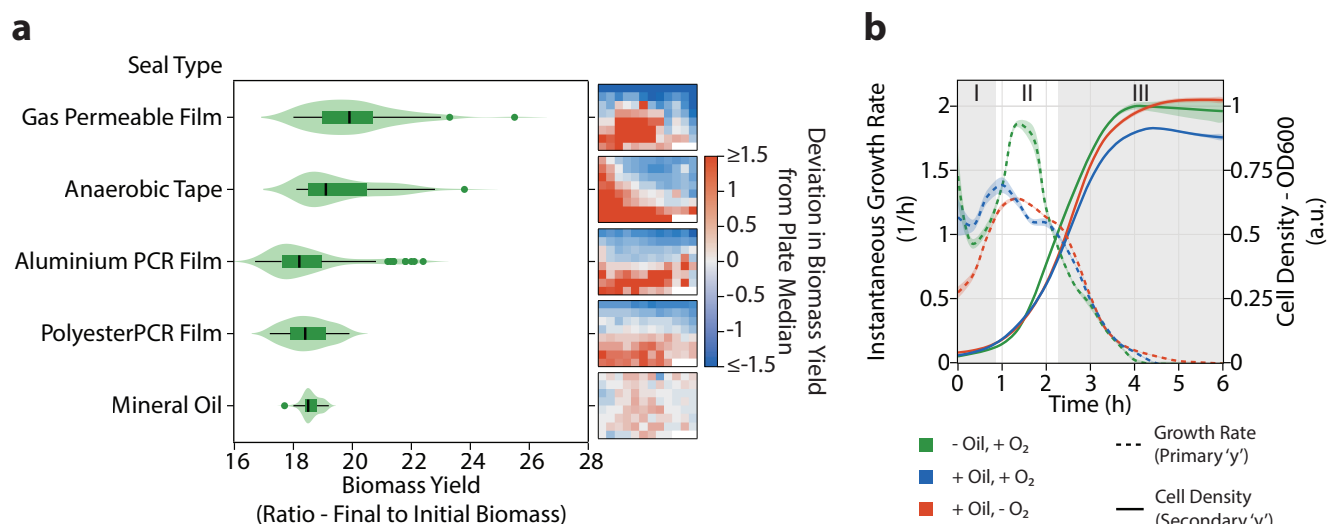


**Figure 5: Establishing anaerobicity in 96-well microplates** **a.** Effectiveness of various seals in preventing oxygen penetration into microplates containing *E. coli* MG1655 in RDM, sealed within an anaerobic chamber. The biomass within each microplate are represented as violin plots. To the right of each violin plot, the distribution of biomass yields are represented as heatmaps showing deviation of the biomass yields from the median biomass yield within that plate. **b.** Time-course showing cell density and instantaneous growth rate of *E. coli* MG1655 in RDM with and without a layer of oil in the presence of oxygen and with a layer of mineral oil inside an anaerobic chamber.

210 we found clear patterns of enhanced growth in certain areas, likely resulting from improper sealing and  
 211 heterogeneous oxygen concentrations (Figure 5a and Supplementary Figure S2). Hence, the use of a film  
 212 would inevitably lead to heterogeneity in cellular phenotypes in addition to increased throughput times  
 213 due to the need for manual sealing of each microplate.

214 Alternatively, a layer of mineral oil (50  $\mu$ L), pipetted on top of the microbial culture in each well offered  
 215 a homogeneous gas exchange profile, evidenced by the tight distribution of biomass yield (Figure 5a and  
 216 Supplementary Figure S2). The mineral oil was also successful at completely eliminating loss of media  
 217 during the fermentation within the anaerobic chamber, restoring the ability to monitor growth accurately  
 218 (Supplementary Figure S3). In order to ensure that the growth profiles of *E. coli* are only affected by the  
 219 resulting oxygen transfer and not directly by the mineral oil, we examined the growth of four different  
 220 strains of *E. coli* with and without the layer of mineral oil, inside and outside the anaerobic chamber  
 221 (Figure 5b and Supplementary Figure S3). We were able to clearly distinguish three different regimes  
 222 in all the growth profiles - (I) an initial regime where dissolved oxygen in the media is used, indicated  
 223 by the relatively higher growth rates of cells grown outside the anaerobic chamber, (II) an intermediate  
 224 regime where the cells without the layer of mineral oil outside the anaerobic chamber are able to grow at  
 225 accelerated rates due to increased oxygen transfer, and (III) a final growth phase where all the cells grow  
 226 at similar rates due to no oxygen transfer due either to high cell densities or to the layer of mineral oil.  
 227 It can be inferred from growth regimes (I) and (III) that the mineral oil does not directly impair or assist  
 228 the growth of the strains but only controls the rate of gas exchange. Hence, it is suitable to maintain  
 229 anoxic growth within an anaerobic chamber for extended durations with minimal loss of media due to  
 230 evaporation.

231 **Case Study 1: Applying the liquid handling platform for an anaerobic enzymatic**  
232 **screen**

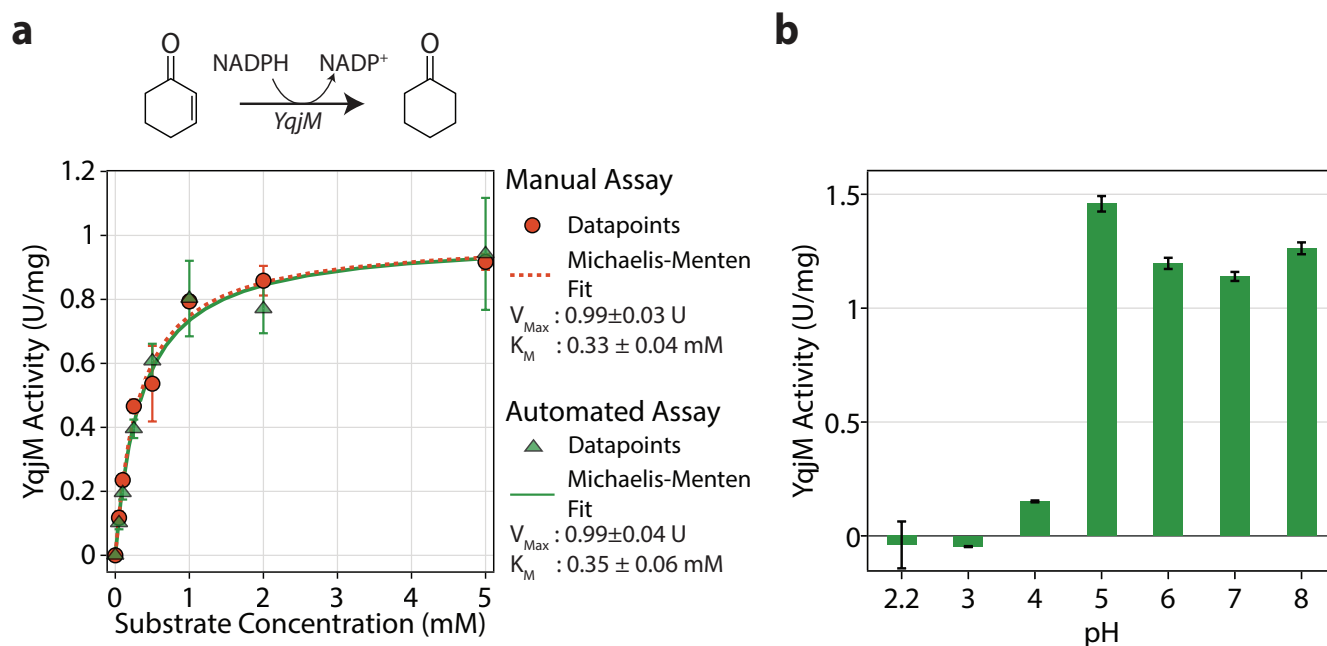


**Figure 6: Anaerobic enzymatic screen a.** Enzymatic activity of YqjM on 2-cyclohexen-1-one determined manually and by the liquid handler. Enzyme activity is represented in units of  $\mu\text{mol}/\text{min}$ . **b.** Effect of pH of the medium on the activity of YqjM on 2-cyclohexen-1-one.

233 As a preliminary validation of our high throughput phenotyping platform, we sought to perform an  
234 anaerobic activity screen of the enoate reductase enzyme YqjM from *Bacillus subtilis* (*Bs*-YqjM). This  
235 enzyme belongs to the family of old yellow enzymes (EC 1.6.99.1) which are broadly known as enoate  
236 reductases. They use non-covalently bound flavin mononucleotide (FMN) to catalyze the reduction of  
237 double bonds found in  $\alpha,\beta$ -unsaturated aldehydes and ketones using NADPH or NADH as electron  
238 donors<sup>13</sup>. The ability of *Bs*-YqjM and other enoate reductases to reduce -ene groups is important for the  
239 catalysis of chemical commodities such as muconic acid to adipic acid (a pre-cursor to nylon). However,  
240 the activity of *Bs*-YqjM enzymatic activity is known to be suppressed in the presence of oxygen under  
241 aerobic conditions due to a prominent background reaction where electrons from NADPH are transferred  
242 to dissolved molecular oxygen in the buffer. In contrast, its activity is markedly increased under anaerobic  
243 conditions where electrons are instead donated to its target -ene substrates<sup>40</sup>. For the 2-cyclohexen-1-one  
244 substrate, *Bs*-YqjM was reported to have a  $K_M$  value of 0.3-0.6 mM under anaerobic conditions created  
245 using a glucose-glucose oxidase system, which consumes the dissolved molecular oxygen in the buffering  
246 solution to simulate completely anaerobic conditions.

247 To demonstrate the use of an automated LiHa platform for performing anaerobic assays, we purified  
248 *Bs*YqjM and assayed its activity for 2-cyclohexen-1-one by monitoring changes in the absorbance at 340  
249 nm due to NADPH oxidation. After calibration of the tips for smaller volumes in the 3-10  $\mu\text{L}$  range, we  
250 observed a  $K_M$  value of  $0.35 \pm 0.06$  mM using the automated platform (Figure 6a). In comparison, we  
251 performed the same assay manually and observed a  $K_M$  value of  $0.33 \pm 0.4$  mM. The similarity of these  
252  $K_M$  values to each other and to published literature values suggested that the LiHa platform could be

253 used to automate the preparation of screens, such as those to determine the optimal pH for maximum  
 254 activity. Towards this end, we determined Bs-YqjM's activity across pH 2.2 – 8 using the liquid handler  
 255 (Figure 6b). We found that BsYqjM operates optimally at pH 5-6, which aligns with previously reported  
 256 results that Bs-YqjM prefers slightly acidic conditions<sup>40</sup>.

257 **Case Study 2: Scaling down anaerobic microbial phenotypes from pH controlled**  
 258 **bioreactors to microplates**

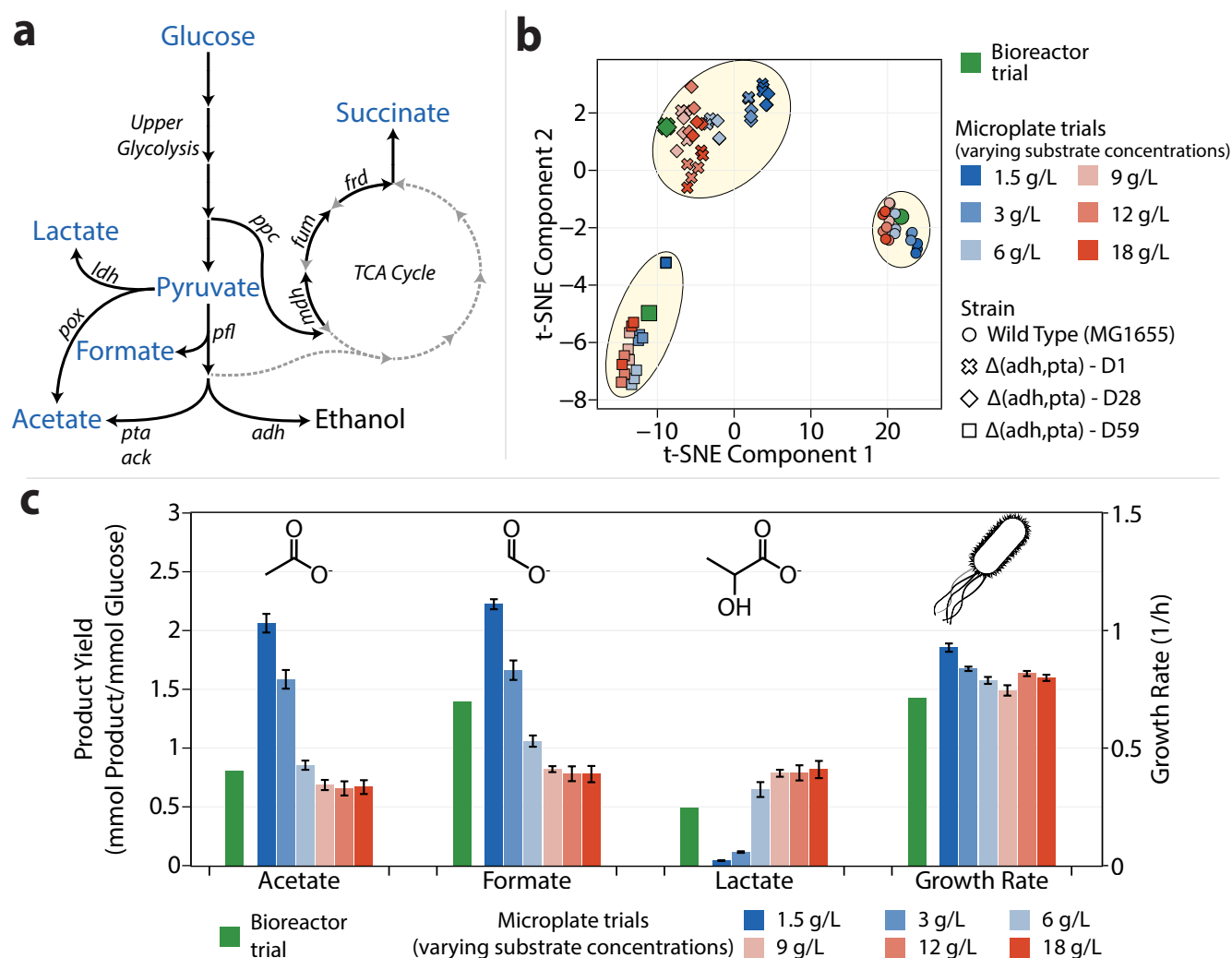


**Figure 7: Comparison of *E. coli*'s anaerobic phenotype in bioreactors and microplates a.** Schematic showing typical fermentation pathways in *E. coli*. Typical products of mixed acid fermentation on glucose are shown in the pathway along with key fermentation reactions shown in italics. The metabolites measured in this study are shown in blue. **b.** Microbial phenotypes reduced to two components through t-distributed stochastic neighbors embedding (t-SNE) performed on the metabolite (acetate, formate, lactate, pyruvate, and succinate) yields and growth rates of *E. coli* strains grown in rich defined media in a bioreactor and microplates with different initial concentrations of substrate (glucose). Cluster boundaries were drawn manually for illustrative purposes. **c.** A comparison of WildType *E. coli*'s growth rate and metabolite yields on glucose obtained from a bench-top 0.5 L bioreactor and 96-well microplates with different initial concentrations of substrate (glucose).

259 Having assessed the efficacy of our system in determining enzyme kinetic parameters under anaerobic  
260 conditions, we wished to investigate the applicability of a fixed-tip liquid handling system for a high-  
261 throughput characterization of microbial phenotypes under anaerobic conditions. While it is possible to  
262 rapidly cultivate microbial strains using our platform, the possible deviation of phenotypes at increasingly  
263 larger scales is a cause for concern, resulting in ambiguity of the strains to be chosen for further screening.  
264 Previous studies examining scaling considerations have primarily investigated the difficulty of improving  
265 oxygen transfer rates within the wells of microplates<sup>25,54</sup>. However, since we are interested only in  
266 anaerobic environments, oxygen transfer rates may not play a key role in determining phenotypes. Rather,  
267 the concentration of substrate, pH, and other media conditions could be the determining factors. Hence, as  
268 a second test case to validate our platform, we investigated the ability to scale-down microbial phenotypes  
269 observed in pH controlled 500 mL bioreactors to 96 well microplates under anaerobic conditions. To  
270 this end, we examined the growth and metabolite profiles of four strains of *E. coli* - MG1655 and  
271 its lactate overproducing deletion mutant, MG1655  $\Delta(adhE,pta)$  at three different stages of adaptive  
272 laboratory evolution (denoted  $\Delta(adhE,pta)$ -D1, D28 and D59 to represent the duration of adaptive  
273 laboratory evolution in days)<sup>14</sup>. These strains were chosen because of the expected difference in their  
274 anaerobic phenotypes. During anaerobic growth, *E. coli* undergoes mixed acid fermentation due to the  
275 non-availability of oxygen as a terminal electron acceptor to produce ATP and regenerate the redox  
276 cofactors NAD and NADP. Instead, *E. coli* produces a mixture of formate, acetate, ethanol, lactate,  
277 and small quantities of other organic acids as terminal fermentation products (Figure 7a), with acetate,  
278 ethanol, and formate being preferred products due to higher energy yields. Due to deletions around  
279 key fermentation reactions involved in acetate and ethanol production (*pta* and *adhE* respectively), the  
280 deletion mutants used in our study are expected to show high lactate yields. Further, because these strains  
281 are products of adaptive laboratory evolution, those strains at a later stage of evolution are expected to  
282 show increased growth rates.

283 To compare the metabolic state of the different strains grown in a bioreactor and microplates, we  
284 calculated the growth rates and yields of five different products of fermentation on glucose towards the end  
285 of the exponential phase of growth (Supplementary Figure S7). The deletion mutants grown in microplates  
286 showed good agreement with the bioreactor phenotype as is, possibly due to the elimination of the most  
287 prominent fermentation modes - acetate and ethanol production. However, the wild type strain showed  
288 pronounced phenotypic differences in the microplate, producing significantly lower levels of formate. It  
289 appeared that more carbon flux was directed towards lactate production than formate production in  
290 the microplates, resulting in less energy efficient fermentation and therefore, reduced growth rates. In  
291 order to eliminate the possibility of residual dissolved oxygen in the media causing aberrant phenotypes  
292 and lower formate yields, we examined the effect of adding the reducing agents - 1 mM cysteine, 1 mM  
293 dithiothreitol (DTT), and 8 mM sodium sulfide to scavenge any residual oxygen and maintain reducing  
294 conditions within the media (Figure 7b and Supplementary Figure S7). Higher concentrations of sodium  
295 sulfide were chosen because previous experiments at the 1mM level showed no visible differences in  
296 the phenotype. To better visualize and compare the overall phenotypic differences resulting from the  
297 different strains and media conditions, we performed a dimensionality reduction of the seven analytes  
298 (growth rate and yields of acetate, formate, lactate, pyruvate, succinate and biomass on glucose) through  
299 principal component analysis (PCA) (Supplementary Figure S6). Upon analysis of the scores of each

300 experimental trial on the first two principal components, the bioreactor trial for the wild-type strain  
301 resulted in phenotypes which could not be replicated in microplates since the bioreactor trials seemed  
302 to be isolated from the clusters formed by the microplate trials. Further, PCA indicated that residual  
303 oxygen may not an issue since the addition of reducing agents did little to alter the phenotypes. Examining  
304 the individual analytes (Figure S7), we found that the addition of cysteine at 1 mM did not alter the  
305 metabolite and growth profiles significantly for any of the strains. The addition of DTT showed a decrease  
306 in the yield of nearly all products including biomass for all strains, indicating that it could be inhibitory to  
307 the cells. Interestingly, the addition of sodium sulfide seemed to push the metabolic state slightly towards  
308 that observed in the bioreactor, with increased growth rates and acetate yields but lower lactate yields.  
309 However, since we did not observe similar phenotypes using the other reducing agents, we hypothesized  
310 that this difference could be due to the basic nature of sodium sulfide, which would result in longer  
311 fermentation times and therefore a different metabolic profile. We confirmed this by growing *E. coli* at a  
312 higher starting pH, resulting in longer fermentation duration, and similar trends in the metabolite yields  
313 and growth rates as observed in the addition of sodium sulfide.

314 Hence, we concluded that our platform resulted in complete anaerobicity of the media and it was  
315 not dissolved oxygen that was affecting the metabolic state of the cells. It appeared that the pH and  
316 consequently, the fermentation duration played a more important role in determining the phenotype of  
317 the wild-type strain, as expected. The implementation of pH control in microplates requires specialized  
318 microplates with base delivery systems or mini-bioreactors, which would greatly increase operational  
319 costs<sup>15,50</sup>. We proposed that varying initial glucose concentrations would offer a crude yet inexpensive  
320 means to alter the duration of fermentation, thereby limiting pH change, and consequently, impact the  
321 phenotypes of all strains. Therefore, we grew the *E. coli* strains with different starting concentrations of  
322 glucose to examine this effect and determine glucose concentrations that allowed the phenotype of the  
323 wild-type strain observed in the bioreactor trial to be replicated in microplates (Figure 7c and Supple-  
324 mentary Figure S9). At high initial glucose concentrations, all strains showed increased lactate yields and  
325 reduced biomass, formate and acetate yields on glucose. Specifically, for the wild type strain, this indi-  
326 cates that a significant portion of the carbon flux is directed towards lactate production with reduced flux  
327 through *pfl*, *pta*, and *adh*, resulting in less efficient fermentation and reduced growth rates. However, at  
328 lower substrate concentrations, the overall fermentation duration and consequently, the pH change during  
329 the fermentation decrease. This results in less overflow of carbon flux towards lactate and increased yields  
330 of biomass, acetate and formate, with almost no lactate and maximal formate, acetate and growth rates  
331 at the lowest concentrations analyzed. Performing the same dimensionality reduction through PCA as  
332 described previously, we found that varying initial glucose concentrations significantly alters the overall  
333 phenotypes exhibited by the cells, as shown by the spread of the scores of each experimental trial in  
334 the principal component space (Supplementary Figure S8). Interestingly, several microplate trials with  
335 overall phenotypes very close to their bioreactor counterparts for each strain were observed. Particularly,  
336 the wild-type strain seemed to be closest to the microplate trial starting with 6 g/L of glucose. The other  
337 strains seemed less impacted by high initial glucose concentrations and showed good agreement with the  
338 bioreactor phenotype even at high glucose concentrations.

339 While these results indicate that phenotypes observed in bioreactors can be reasonably replicated in  
340 microplates by varying initial substrate concentrations, the exact value for each strain may not be the

341 same, as seen here. Further, the optimal glucose concentration for each strain cannot be determined a  
342 priori, which may lead to ambiguity in determining better performing strains to be chosen for scale up.  
343 Hence, we wished to investigate dimensionality reduction techniques, using which strains showing simi-  
344 larities at the bioreactor scale could be clustered together while segregating those that showed significant  
345 differences. Our dataset from the experiments varying initial glucose concentrations was ideal for this  
346 purpose since we observed an array of different phenotypes at the microplate scale for the same strain.  
347 Further, the mutant strains -  $\Delta(\text{adh, pta})\text{-D1}$  and  $\Delta(\text{adh, pta})\text{-D28}$  showed very similar phenotypes at  
348 the bioreactor scale. As seen previously (Supplementary Figure S8), principal component analysis was  
349 only partially successful in this effort - while most trials with the D1 and D28 strain exp appeared in the  
350 same cluster, trials with the D59 strain also occurred very close to them. Moreover, the wild-type strains  
351 could not form a single cluster, possibly due to the large variability in the metabolite yields. Hence, a  
352 two-dimensional PCA alone cannot be used to determine strains that would show similar performance  
353 at larger scales, possibly due to omitting the variance explained by the other principal components. A  
354 relatively new dimensionality reduction algorithm - t-distributed stochastic neighbors embedding, which  
355 recreates the probability distribution of entities in a higher dimensional space to two dimensions, has been  
356 found to be successful at clustering similar entities when a large number of dimensions are involved<sup>49</sup>.  
357 Particularly, it has found use in analyzing single cell transcriptomic data. Eventhough our dataset is  
358 comprised of only 6 dimensions i.e. the yields of five metabolites and the growth rates, we proposed that  
359 tSNE could potentially be successful at clustering similar performing strains in a reduced dimensional  
360 space, particularly due to its use of non-linear dimensionality reduction. Remarkably, a tSNE model  
361 fit to our glucose varying data showed near perfect clustering of strains showing similar performance at  
362 the bioreactor scale (Figure 7b). Specifically, all microplate trials from the wild-type strains and the  
363  $\Delta(\text{adh, pta})\text{-D59}$  strain were resolved into their individual clusters in spite of the visible differences in  
364 the phenotypes of individual trials. The two mutants  $\Delta(\text{adh, pta})\text{-D1}$  and  $\Delta(\text{adh, pta})\text{-D28}$  that showed  
365 similar performance at the bioreactor scale were resolved into a single cluster. These results indicate  
366 that tSNE could be used effectively to shortlist strains for analysis at larger scales, since it is able to  
367 effectively segregate strains showing markedly different phenotypes. Therefore, while initial glucose con-  
368 centrations affect the phenotypes of microbial strains at the microplate scale significantly, the use of  
369 dimensionality reduction techniques such as tSNE could be used to resolve these differences and identify  
370 overall phenotypic differences between strains.

## 371 Conclusions

372 We have seen that our automated platform is able to rapidly and effectively set up microplate experi-  
373 ments to phenotype enzymes and microbial strains. The automation of such routine metabolic engineering  
374 workflows greatly expands the number of different strains/enzymes and media conditions that can be ex-  
375 amined, resulting in large experimental datasets that can assist strain design. With machine learning  
376 applications in metabolic engineering becoming more prevalent, there is an urgent need to develop tools  
377 and protocols for accurate and reproducible phenotyping strains and enzymes at smaller scales. Auto-  
378 mated systems are uniquely suited for this task since they eliminate human error and require standardized  
379 protocols to function. Furthermore, recent efforts toward developing robot programming languages that

380 allow for the development of cross-platform protocols enable relatively easy implementation of complex  
381 laboratory workflows<sup>33,34,55</sup>.

382 While automation can enhance experimental throughput, conducting experiments at accelerated rates  
383 also increases operational costs and the amount of laboratory waste generated due to the number of pipette  
384 tips and other labware used. Laboratory plastic waste has become a major concern in the current era  
385 of high-throughput experimentation<sup>3,30,48</sup>. It is quite ironic that the same research labs that work on  
386 developing microbes for sustainable production of chemicals end up generating several million tonnes of  
387 plastic waste in the process. Through the development of effective and fast decontamination protocols,  
388 we eliminated the need for plastic pipette tips while maintaining experimental throughput. Disregarding  
389 repeated and failed experiments, we estimate that nearly 4000 pipette tips would be required to complete  
390 the two case studies examined in this work if they were done manually or using a disposable tip liquid  
391 handling platform. Further, the automated pipette calibration protocol developed here enables the quick  
392 setup of a broad range of liquid handling systems for different pipetting programs and would also assist  
393 in routine maintenance without the need for additional expensive equipment.

394 One concern with phenotyping microbial strains in microplates is the inability to replicate the mix-  
395 ing regimes, oxygen transfer and other physical characteristics of fermentation observed in larger pH  
396 controlled bioreactors. These considerations are better addressed in miniature bioreactors that have  
397 been designed to be small scale replicas of bench-top bioreactors. Nevertheless, by leveraging the en-  
398 hanced throughput of microplate experiments, we were able to analyze the effect of a large number of  
399 media conditions on the cellular phenotypes in a relatively short period of time. Consequently, we were  
400 able to identify glucose concentrations that restricted fermentation durations and thereby, reasonably  
401 reproduce bioreactor phenotypes in microtiter plates under anaerobic conditions. Furthermore, modern  
402 dimensionality reduction and data visualization techniques such as tSNE could be used in conjunction  
403 with microplate experiments as scale-down models to assist in choosing strains for scale-up. We believe  
404 that since microplates offer higher experimental throughput at very low costs, our platform will serve  
405 as an effective and representative screen before moving on to larger scales. Furthermore, integration  
406 of our data analysis pipeline - IMPACT with the strain testing pipeline has enabled the visualization  
407 and analysis of large datasets that emerge as a consequence of our platform, and will accelerate future  
408 strain design endeavours. While successful at anaerobic phenotyping, we believe that the experimental  
409 protocols described in this study are broadly applicable to various liquid handling platforms for a wide  
410 range of applications and this work will assist the development of sustainable automated high throughput  
411 experimental platforms.

## 412 **Materials & Methods**

### 413 **Enzymes, Strains and Experimental Medium**

414 Wild type *Escherichia coli* strain K-12 MG1655 was used to detect contamination during the development  
415 of our decontamination protocol. The wild type *Escherichia coli* strain K-12 MG1655 and its mutants  
416 harboring deletions of the genes *adhE* and *pta* at three different stages of adaptive laboratory evolution<sup>14</sup>  
417 (denoted  $\Delta(\text{adhE, pta})\text{-D1}$ ,  $\Delta(\text{adhE, pta})\text{-D28}$ , and  $\Delta(\text{adhE, pta})\text{-D59}$  to reflect duration of adaptive  
418 laboratory evolution in days) were used to examine the efficacy of our phenotyping platform. The enoate

419 reductase enzyme yqjM (UniProt: P54550) from *Bacillus subtilis* strain 168 was used for the anaerobic  
420 screen.

421 Lysogeny Broth (LB) media was used to prepare bacterial starter cultures in all cases. Strain phe-  
422 notyping experiments were conducted in a rich defined medium (RDM) composed of a carbon source  
423 (D-glucose at various concentrations), salts (3.5 g/L  $\text{KH}_2\text{PO}_4$ , 5 g/L  $\text{K}_2\text{HPO}_4$ , 3.5 g/L  $(\text{NH}_4)_2\text{HPO}_4$ ,  
424 1 mM  $\text{MgSO}_4$ , 0.1mM  $\text{CaCl}_2$ ), 1 mM 3-morpholinopropane-1-sulfonic acid (MOPS), amino acid supple-  
425 ments (0.8 mM alanine, 5.2 mM arginine, 0.4 mM asparagine, 0.4 mM aspartate, 0.1 mM cysteine, 0.6 mM  
426 glutamate, 0.6 mM glutamine, 0.8 mM glycine, 0.2 mM histidine, 0.4 mM isoleucine, 0.8 mM leucine, 0.4  
427 mM lysine, 0.2 mM methionine, 0.4 mM phenylalanine, 0.4 mM proline, 10 mM serine, 0.4 mM threo-  
428 nine, 0.1 mM tryptophan, 0.2 mM tyrosine, and 0.6 mM valine), nucleotide supplements (0.1 mM each  
429 of adenine, cytosine, guanine, and uracil), and vitamin supplements (0.01 mM each of thiamine, calcium  
430 pantothenate, *p*-aminobenzoic acid, *p*-hydroxybenzoic acid, and 2,3-dihydroxybenzoic acid) - adapted  
431 from the defined media composition described previously<sup>36</sup>. All media components were sterilized either  
432 by autoclaving or filter sterilization. Stocks of cysteine, dithiothreitol (DTT), and sodium sulfide for use  
433 as reducing agents to maintain anaerobicity in the media were prepared at a concentration of 0.2 M. The  
434 stocks were sparged gaseous nitrogen through the solutions for 15 minutes to eliminate dissolved oxygen,  
435 followed by sterilization.

436 12% sodium hypochlorite (Bioshop SYP001.1) and 95% ethanol were diluted to required concentra-  
437 tions to prepare disinfectants for the decontamination protocol. Aqueous solutions of potassium dichro-  
438 mate (0.4 mM, 1mM, and 2mM) were prepared to detect pipetting accuracy and calibrate the liquid  
439 handling system. The polyurethane gas permeable film (Diversified Biotech BEM-1), polyester PCR  
440 film (Bio-Rad MSB1001), and aluminized foil (Bio-Rad MSF1001) were used to seal 96 well microplates  
441 (Corning 353072) containing *E. coli* cultures to investigate anaerobicity. Mineral oil (BioShop MIN444)  
442 was used to prevent evaporation in anaerobic chambers where required.

## 443 High throughput phenotyping platform

444 The phenotyping platform described in this study was comprised of a Tecan Freedom Evo 100 base fitted  
445 with a Tecan fixed-tip liquid LiHa (liquid handling) arm, a Tecan RoMa (robotic manipulator) arm,  
446 a QInstruments Bioshake 3000-T microplate heater-shaker, an Agilent microplate centrifuge, a Tecan  
447 Infinite M200 plate reader, and a Tecan Te-VacS vacuum filtration module. Communication with the  
448 various modules and all automation scripts were set up on Tecan's EvoWare 2.7 platform.

## 449 Enzyme Purification for Anaerobic Screen

450 The gene encoding yqjM was cloned under the T7 promoter in-frame with an N-terminal 6x HisTag of the  
451 p15TvL expression vector (AddGene: 26093) using the In-Fusion®HD EcoDry kit, and then transformed  
452 into LOBSTR BL21(DE3) *Escherichia coli*. Starter cultures for yqjM were grown from glycerol stock in  
453 lysogeny broth (LB) media with ampicillin (100  $\mu\text{g}/\text{mL}$ ) for 16 hrs at 37 °C with shaking. Then, expression  
454 cultures were started in 1L Terrific Broth media with ampicillin (100  $\mu\text{g}/\text{mL}$ ) and a 1% v/v inoculant of  
455 the starter culture, followed by growth for 4 hrs at 37 °C and induction with 0.4 mM IPTG. The expression  
456 culture was then transferred to 16 °C and grown for 16 hrs with shaking, pelleted with centrifugation, and



457 transferred to vials for one freeze-thaw cycle at  $-20^{\circ}\text{C}$ . Frozen cell pellets were thawed and resuspended  
458 in binding buffer (10 mM HEPES, 500 mM NaCl, 5 mM imidazole, pH 7.2) to a final volume of 50 mL,  
459 followed by addition of 0.25 g lysozyme. Cell pellet mixtures were sonicated for 25 min and clarified  
460 by centrifugation. The supernatant was applied to a cobalt-charged NTA resin pre-equilibrated with  
461 binding buffer in a gravity-column set-up. Bound proteins were cleansed with 120 mL of wash buffer  
462 (10 mM HEPES, 500 mM NaCl, 25 mM imidazole, pH 7.2) and collected with 4 mL elution buffer (10  
463 mM HEPES, 500 mM NaCl, 250 mM imidazole, pH 7.2). Protein concentrations were determined by  
464 Bradford assay to be 4.3 mg/mL (120  $\mu\text{M}$ ), and protein purity was determined by SDS-PAGE analysis  
465 and densitometry to be 99%. A molar equivalent of flavin mononucleotide (FMN) was loaded into YqjM  
466 prior to transfer into a 10 kDa MWCO dialysis bag for dialysis in 1 L dialysis buffer (40 mM HEPES,  
467 pH 7.5) at  $4^{\circ}\text{C}$  with gentle stirring for 24 hrs. YqjM was then flash frozen drop-wise in liquid nitrogen  
468 before storage at  $-80^{\circ}\text{C}$ .

### 469 **NADPH Assay for Determination of Anaerobic YqjM Activity**

470 The glucose oxidase type VII-S from *Aspergillus niger* was used to remove oxygen from enzyme screen  
471 reactions using D-glucose as the substrate. Working concentrations of 2-cyclohexen-1-one (substrate),  
472  $\beta$ -NADPH tetrasodium salt (indicator), glucose oxidase type VII-S from *Aspergillus niger*, and glucose  
473 were prepared in 40 mM HEPES at a pH of 7.5 to assay yqjM activity. Assays were set up in a 96 well  
474 microplate using the liquid handler and consisted of 0.15 mM NADPH, 10 u/mL glucose oxidase, 20 mM  
475 glucose, and 15 nM YqjM. The substrate, 2-cyclohexen-1-one was then added at required concentrations  
476 along with the activity buffer to make each assay up to a volume of 200  $\mu\text{L}$ . The pH gradients were  
477 prepared using McIlvaine buffers with appropriate ratios of 0.2 M  $\text{Na}_2\text{HPO}_4$  and 0.1 M citric acid which  
478 replaced the activity buffer. Salt gradients were prepared by adding appropriate concentrations of NaCl  
479 and KCl to the activity buffer.

480 YqjM activity was determined by measuring NADPH concentrations in triplicate using kinetic reads  
481 performed using a Molecular Devices SpectraMax M2 spectrophotometer at  $35^{\circ}\text{C}$  at an absorbance wave-  
482 length of 340 nm with shaking before and in between kinetic reads. The volumetric activities ( $\mu\text{mol}$   
483  $\text{min}^{-1} \text{mg}^{-1}$ ) were calculated using NADPH's extinction coefficient of  $6.3 \text{ mM}^{-1} \text{ cm}^{-1}$  and a height of  
484 0.56 cm. The obtained activity data was fit to a Michaelis-Menten curve to obtain  $K_M$  and  $V_{Max}$  through  
485 non-linear regression using optimization tools in the python package - scipy<sup>53</sup>.

### 486 **Determination of microbial phenotypes in microplates**

487 *E. coli* strains streaked on LB-agar plates were used to prepare starter cultures for the scaled down  
488 phenotyping experiments. The strains were inoculated in LB media supplemented with 1% glucose in  
489 96 well microplates and grown overnight at  $37^{\circ}\text{C}$  with constant shaking at 250 rpm. Glucose was added  
490 to the starter cultures to eliminate the need for an intermediate adaptation culture in the experimental  
491 media - RDM (Supplementary Figure S4). The microplates containing the overnight precultures were  
492 then transferred to the liquid handling platform for processing. All following steps were automated on  
493 the liquid handling platform.

494 First, to remove traces of fermentation products and spent media from the strains, the pre-cultures

495 were harvested by centrifugation at 3000 g for 10 minutes and washed with RDM lacking carbon source  
496 2 times before being resuspended in the experimental RDM medium consisting of the carbon source  
497 and any required supplements. Then, the cell density of each well was determined by measuring the  
498 absorbance at a wavelength at 600 nm on a Tecan Infinite M200 plate reader and cells were then diluted  
499 to a cell density of 0.05 with appropriate media to a final volume of 150  $\mu$ L to normalize all wells to the  
500 same starting OD.

501 After this, the plate was removed from the liquid handling platform, taken through cycles of vacuum  
502 and flushing with nitrogen gas, and transferred into an anaerobic chamber filled with N<sub>2</sub> gas. The  
503 cultures were then covered with a 50 $\mu$ L layer of laboratory grade mineral oil (BioShop MIN444) to  
504 prevent evaporation. To ensure anaerobic conditions throughout the fermentation, the cells were grown  
505 within the anaerobic chamber at 37°C and constant shaking in a Molecular Devices SpectraMax M2  
506 platereader which also recorded the cell density periodically.

507 After the cells finished growing (about 8h), the microplate was removed from the anaerobic chamber  
508 and transferred to the liquid handler for HPLC sample preparation. The liquid handling platform was  
509 programmed to pipette the samples onto a 0.2  $\mu$ m filter plate (Millipore MSGVN2210) for filtration. Sam-  
510 ples were filtered at 400 psi for 60 s into a sample collection plate. Fermentation products were separated  
511 by passing the samples through an Aminex HPX-87H cation exchange column (BioRad 1250140) at a  
512 flow rate of 0.6 mL/min with 5mM H<sub>2</sub>SO<sub>4</sub> as the mobile phase and 60°C column temperature. Metabolite  
513 concentrations were determined by monitoring the refractive index and UV absorbance (at 210 nm, 254  
514 nm) of the eluent. The chromatograms were integrated using Chromeleon v7.

## 515 **Determination of microbial phenotypes in pH controlled bioreactors**

516 *E. coli* strains streaked on LB-agar plates were used to prepare starter cultures by inoculation into 5 mL  
517 LB + 1% glucose. Cultures were then transferred to 50 mL sealed Falcon tubes for oxygen limitation. Af-  
518 ter overnight growth, cells were washed 3 times with RDM lacking carbon source before being transferred  
519 to 500 mL bioreactors (Applikon Mini) with 300mL of RDM with a glucose concentration of 2%. The  
520 media in the bioreactors was maintained anaerobic by sparging with nitrogen gas. pH was maintained  
521 at 7 within the bioreactor by continuous control using 10 M NaOH and the temperature was maintained  
522 at 37 °C. Samples for cell density and metabolite concentration measurements were withdrawn from the  
523 bioreactor periodically. Cell density was determined by measuring absorbance at 600 nm on a spectropho-  
524 tometer (Thermo Scientific GENESYS20). Metabolite concentrations were determined through HPLC  
525 as described in the previous section after filtering the samples through 0.2  $\mu$ m nylon filters.

## 526 **Data Analysis**

527 Data analyses for all sections were conducted using Python on Jupyter notebooks. The jupyter notebooks  
528 used to generate figures and process data in this work are available on Github<sup>42</sup>. The python based data  
529 analysis library - pandas and plotting library - plotly were used extensively for all data analysis and  
530 visualization pipelines in this work<sup>21,38</sup>.

531 Microbial phenotypic data and growth curves were analyzed using the IMPACT Framework<sup>51</sup>. For the  
532 microbial phenotyping experiments, since time-course metabolite concentrations could not be obtained

533 for the microplate trials, end-point metabolite concentrations were used to calculate yields. Hence,  
534 for a fair comparison with the microplate trials, yields for the bioreactor trials were calculated from  
535 metabolite concentrations obtained near the end of the exponential phase of growth. Growth rates  
536 for both bioreactor and microplate trials were determined from only the exponential phase of growth  
537 and were calculated as the specific biomass productivity (i.e.  $1/[X]*d[X]/dt$  where  $[X]$  is the biomass  
538 concentration) and averaged over the required time-period. The sci-kit learn library was used perform  
539 principal component analysis (PCA) to reduce the dimensionality of scaled phenotype data (growth rates  
540 and yields of acetate, formate, lactate, pyruvate, and succinate on glucose) and enable easier phenotypic  
541 comparisons<sup>39</sup>. A number of components that explained at least 90% of the variance in the phenotypic  
542 data was chosen for PCA. Phenotypic data was scaled to unit variance and zero mean prior to PCA.  
543 Similarly, t-distributed stochastic neighbours embedding was also implemented from the sci-kit learn  
544 library. A perplexity that resulted in the most robust embedding was determined after iterating through  
545 several values. The learning rate ( $\epsilon$ ) that minimized the Kullback–Leibler divergence of the input data  
546 distribution and the resulting distribution was used. Regardless, other values of perplexity and learning  
547 rate resulted in similar results when an optimal solution was achieved.

## 548 **Supporting Information**

549 Supplementary Table S1 in the Supporting Information contains details of reaction abbreviations used in  
550 Figure 7a. Supplementary Figures S1-S9 of Supporting Information are figures that have been referenced  
551 in the manuscript

## 552 **Author Contributions**

553 KR helped formulate the study, developed automation protocols, performed experiments, developed the  
554 codebase, and wrote and edited the manuscript. NV helped formulate the study, developed automation  
555 protocols, and reviewed the manuscript. PD performed enzyme kinetic screens and wrote the manuscript.  
556 SG performed experiments. AY supervised the work and reviewed the manuscript. RM helped formulate  
557 the study, supervised the work and reviewed the manuscript.

## 558 **Acknowledgements**

559 The authors thank Prof. Stephen Fong (Virginia Commonwealth University, USA) for providing the lactic  
560 acid overproducing mutants used in this study. We also thank Prof. Po-Hsiang Wang (National Central  
561 University, Taiwan) for insightful discussions about maintaining anaerobicity in cell cultures. This work  
562 was financially supported by grants from Genome Canada, The Ontario Ministry for Research, Innovation,  
563 and Science, and the National Sciences and Engineering Research Council of Canada. KR would like to  
564 acknowledge funding from an Ontario Trillium Scholarship and a Mitacs Globalink Fellowship.

## 565 References

- 566 [1] Bessemans, L., Jully, V., de Raikem, C., Albanese, M., Moniotte, N., Silversmet, P., and Lemoine,  
567 D. (2016). Automated gravimetric calibration to optimize the accuracy and precision of tecan freedom  
568 evo liquid handler. *Journal of Laboratory Automation*, 21(5):693–705. PMID: 26905719.
- 569 [2] Betts, J. I. and Baganz, F. (2006). Miniature bioreactors: Current practices and future opportunities.  
570 *Microbial Cell Factories*, 5:1–14.
- 571 [3] Bistulfi, G. (2013). Sustainability: Reduce, reuse and recycle lab waste.
- 572 [4] Burgard, A. P., Pharkya, P., and Maranas, C. D. (2003). OptKnock: A Bilevel Programming Frame-  
573 work for Identifying Gene Knockout Strategies for Microbial Strain Optimization. *Biotechnology and*  
574 *Bioengineering*, 84(6):647–657.
- 575 [5] C. C. Shih, S., Goyal, G., W. Kim, P., Koutsoubelis, N., D. Keasling, J., D. Adams, P., J. Hillson,  
576 N., and K. Singh, A. (2015). A Versatile Microfluidic Device for Automating Synthetic Biology. *ACS*  
577 *Synthetic Biology*, 4(10):1151–1164.
- 578 [6] Carbonell, P., Radivojevic, T., and García Martín, H. (2019). Opportunities at the Intersection of  
579 Synthetic Biology, Machine Learning, and Automation. *ACS Synthetic Biology*, 8(7):1474–1477.
- 580 [7] Chory, E. J., Gretton, D. W., DeBenedictis, E. A., and Esvelt, K. M. (2021). Enabling high-  
581 throughput biology with flexible open-source automation. *Molecular Systems Biology*, 17(3):e9942.
- 582 [8] Crater, J. S. and Lievense, J. C. (2018). Scale-up of industrial microbial processes. *FEMS Microbiology*  
583 *Letters*, 365(13). fny138.
- 584 [9] Dharmadi, Y., Murarka, A., and Gonzalez, R. (2006). Anaerobic fermentation of glycerol by es-  
585 cherichia coli: A new platform for metabolic engineering. *Biotechnology and Bioengineering*, 94(5):821–  
586 829.
- 587 [10] Duetz, W. A. (2007). Microtiter plates as mini-bioreactors: miniaturization of fermentation methods.  
588 *Trends in Microbiology*, 15(10):469–475.
- 589 [11] Edwards, J. S., Ibarra, R. U., and Palsson, B. O. (2001). In silico predictions of Escherichia coli  
590 metabolic capabilities are consistent with experimental data. *Nature Biotechnology*, 19(2):125–130.
- 591 [12] Englander, S., Calhoun, D. B., and Englander, J. J. (1987). Biochemistry without oxygen. *Analytical*  
592 *Biochemistry*, 161(2):300–306.
- 593 [13] Fitzpatrick, T. B., Amrhein, N., and Macheroux, P. (2003). Characterization of yqjm, an old yellow  
594 enzyme homolog from bacillus subtilis involved in the oxidative stress response\*. *Journal of Biological*  
595 *Chemistry*, 278(22):19891–19897.
- 596 [14] Fong, S. S., Burgard, A. P., Herring, C. D., Knight, E. M., Blattner, F. R., Maranas, C. D., and  
597 Palsson, B. O. (2005). In silico design and adaptive evolution of Escherichia coli for production of  
598 lactic acid. *Biotechnology and bioengineering*, 91(5):643–648.

- 599 [15] Funke, M., Buchenauer, A., Schnakenberg, U., Mokwa, W., Diederichs, S., Mertens, A., Müller, C.,  
600 Kensy, F., and Büchs, J. (2010). Microfluidic biolector—microfluidic bioprocess control in microtiter  
601 plates. *Biotechnology and Bioengineering*, 107(3):497–505.
- 602 [16] Gibson, D. G., Young, L., Chuang, R.-Y., Venter, J. C., Hutchison, C. A., and Smith, H. O. (2009).  
603 Enzymatic assembly of DNA molecules up to several hundred kilobases. *Nature Methods*, 6(5):343–345.
- 604 [17] Haby, B., Hans, S., Anane, E., Sawatzki, A., Krausch, N., Neubauer, P., and Bournazou, M. N. C.  
605 (2019). Integrated robotic mini bioreactor platform for automated, parallel microbial cultivation with  
606 online data handling and process control. *SLAS TECHNOLOGY: Translating Life Sciences Innovation*,  
607 24(6):569–582. PMID: 31288593.
- 608 [18] Hillson, N., Caddick, M., Cai, Y., Carrasco, J. A., Chang, M. W., Curach, N. C., Bell, D. J., Le  
609 Feuvre, R., Friedman, D. C., Fu, X., Gold, N. D., Herrgård, M. J., Holowko, M. B., Johnson, J. R.,  
610 Johnson, R. A., Keasling, J. D., Kitney, R. I., Kondo, A., Liu, C., Martin, V. J., Menolascina, F.,  
611 Ogino, C., Patron, N. J., Pavan, M., Poh, C. L., Pretorius, I. S., Rosser, S. J., Scrutton, N. S., Storch,  
612 M., Tekotte, H., Travník, E., Vickers, C. E., Yew, W. S., Yuan, Y., Zhao, H., and Freemont, P. S.  
613 (2019). Building a global alliance of biofoundries.
- 614 [19] Holland, I. and Davies, J. A. (2020). Automation in the life science research laboratory. *Frontiers*  
615 *in Bioengineering and Biotechnology*, 8:1326.
- 616 [20] Huber, R., Ritter, D., Hering, T., Hillmer, A.-K., Kensy, F., Müller, C., Wang, L., and Büchs, J.  
617 (2009). Robo-Lector – a novel platform for automated high-throughput cultivations in microtiter plates  
618 with high information content. *Microbial Cell Factories*, 8(1):42.
- 619 [21] Inc., P. T. (2015). Collaborative data science.
- 620 [22] ISO 8655-2:2002 (2002). Piston-operated volumetric apparatus — Part 2: Piston pipettes. Standard,  
621 International Organization for Standardization, Geneva, CH.
- 622 [23] Janzen, N. H., Striedner, G., Jarmer, J., Voigtmann, M., Abad, S., and Reinisch, D. (2019). Im-  
623 plementation of a Fully Automated Microbial Cultivation Platform for Strain and Process Screening.  
624 *Biotechnology Journal*, 14(10):1800625.
- 625 [24] Julleson, D., David, F., Pfeleger, B., and Nielsen, J. (2015). Impact of synthetic biology and metabolic  
626 engineering on industrial production of fine chemicals. *Biotechnology Advances*, 33(7):1395–1402.
- 627 [25] Kensy, F., Zang, E., Faulhammer, C., Tan, R. K., and Büchs, J. (2009). Validation of a high-  
628 throughput fermentation system based on online monitoring of biomass and fluorescence in continuously  
629 shaken microtiter plates. *Microbial Cell Factories*, 8:1–17.
- 630 [26] Knepper, A., Heiser, M., Glauche, F., and Neubauer, P. (2014). Robotic Platform for Parallelized  
631 Cultivation and Monitoring of Microbial Growth Parameters in Microwell Plates. *Journal of Laboratory*  
632 *Automation*, 19(6):593–601.

- 633 [27] Kok, S. D., Stanton, L. H., Slaby, T., Durot, M., Holmes, V. F., Patel, K. G., Platt, D., Shapland,  
634 E. B., Serber, Z., Dean, J., Newman, J. D., and Chandran, S. S. (2014). Rapid and reliable DNA  
635 assembly via ligase cycling reaction. *ACS Synthetic Biology*, 3(2):97–106.
- 636 [28] Kong, F., Yuan, L., Zheng, Y. F., and Chen, W. (2012). Automatic liquid handling for life science:  
637 A critical review of the current state of the art.
- 638 [29] Lattermann, C. and Büchs, J. (2015). Microscale and miniscale fermentation and screening. *Current*  
639 *Opinion in Biotechnology*, 35:1–6. Chemical biotechnology • Pharmaceutical biotechnology.
- 640 [30] Laura Howes (2019). Reducing plastic use in the lab. *CE&EN Global Enterprise*, 97(43):22–24.
- 641 [31] Lawson, C. E., Martí, J. M., Radivojevic, T., Jonnalagadda, S. V. R., Gentz, R., Hillson, N. J.,  
642 Peisert, S., Kim, J., Simmons, B. A., Petzold, C. J., Singer, S. W., Mukhopadhyay, A., Tanjore, D.,  
643 Dunn, J. G., and Garcia Martin, H. (2021). Machine learning for metabolic engineering: A review.  
644 *Metabolic Engineering*, 63:34–60. Tools and Strategies of Metabolic Engineering.
- 645 [32] Lee, S. Y., Kim, H. U., Chae, T. U., Cho, J. S., Kim, J. W., Shin, J. H., Kim, D. I., Ko, Y. S., Jang,  
646 W. D., and Jang, Y. S. (2019). A comprehensive metabolic map for production of bio-based chemicals.  
647 *Nature Catalysis*, 2(1):18–33.
- 648 [33] Linshiz, G., Stawski, N., Goyal, G., Bi, C., Poust, S., Sharma, M., Mutalik, V., D. Keasling, J.,  
649 and J. Hillson, N. (2014). PR-PR: Cross-Platform Laboratory Automation System. *ACS Synthetic*  
650 *Biology*, 3(8):515–524.
- 651 [34] Linshiz, G., Stawski, N., Poust, S., Bi, C., D. Keasling, J., and J. Hillson, N. (2012). PaR-PaR  
652 Laboratory Automation Platform. *ACS Synthetic Biology*, 2(5):216–222.
- 653 [35] Monk, J., Koza, A., Campodonico, M., Machado, D., Seoane, J., Palsson, B., Herrgård, M., and  
654 Feist, A. (2016). Multi-omics quantification of species variation of escherichia coli links molecular  
655 features with strain phenotypes. *Cell Systems*, 3(3):238–251.e12.
- 656 [36] Neidhardt, F. C., Bloch, P. L., and Smith, D. F. (1974). Culture medium for enterobacteria. *Journal*  
657 *of Bacteriology*, 119(3):736–747.
- 658 [37] Oberortner, E., Cheng, J.-F., J. Hillson, N., and Deutsch, S. (2016). Streamlining the Design-to-Build  
659 Transition with Build-Optimization Software Tools. *ACS Synthetic Biology*, 6(3):485–496.
- 660 [38] pandas development team, T. (2020). pandas-dev/pandas: Pandas.
- 661 [39] Pedregosa, F., Varoquaux, G., Gramfort, A., Michel, V., Thirion, B., Grisel, O., Blondel, M.,  
662 Prettenhofer, P., Weiss, R., Dubourg, V., Vanderplas, J., Passos, A., Cournapeau, D., Brucher, M.,  
663 Perrot, M., and Duchesnay, E. (2011). Scikit-learn: Machine learning in Python. *Journal of Machine*  
664 *Learning Research*, 12:2825–2830.
- 665 [40] Pesic, M., Fernández-Fueyo, E., and Hollmann, F. (2017). Characterization of the old yellow enzyme  
666 homolog from bacillus subtilis (yqjm). *ChemistrySelect*, 2(13):3866–3871.

- 667 [41] Radivojević, T., Costello, Z., Workman, K., and Garcia Martin, H. (2020). A machine learning  
668 Automated Recommendation Tool for synthetic biology. *Nature Communications*, 11(1):1–14.
- 669 [42] Raj, K., Venayak, N., Diep, P., Golla, S. A., Yakunin, A. F., and Mahadevan, R. (2020a). Automated  
670 scaledown GitHub repository. Available from: [https://github.com/lmse/automated\\_scaledown](https://github.com/lmse/automated_scaledown).  
671 Accessed 3 May 2021.
- 672 [43] Raj, K., Venayak, N., and Mahadevan, R. (2020b). Novel two-stage processes for optimal chemical  
673 production in microbes. *Metabolic Engineering*, 62:186–197.
- 674 [44] Rohe, P., Venkanna, D., Kleine, B., Freudl, R., and Oldiges, M. (2012). An automated workflow  
675 for enhancing microbial bioprocess optimization on a novel microbioreactor platform. *Microbial Cell*  
676 *Factories*, 11:144.
- 677 [45] Stangegaard, M., Hansen, A. J., Frøslev, T. G., and Morling, N. (2011). A Simple Method for  
678 Validation and Verification of Pipettes Mounted on Automated Liquid Handlers. *Journal of Laboratory*  
679 *Automation*, 16(5):381–386.
- 680 [46] Tegally, H., San, J. E., Giandhari, J., and de Oliveira, T. (2020). Unlocking the efficiency of genomics  
681 laboratories with robotic liquid-handling.
- 682 [47] Unthan, S., Radek, A., Wiechert, W., Oldiges, M., and Noack, S. (2015). Bioprocess automation on a  
683 Mini Pilot Plant enables fast quantitative microbial phenotyping. *Microbial Cell Factories*, 14(1):1–11.
- 684 [48] Urbina, M. A., Watts, A. J., and Reardon, E. E. (2015). Environment: Labs should cut plastic waste  
685 too.
- 686 [49] Van Der Maaten, L. and Hinton, G. (2008). Visualizing Data using t-SNE. Technical report.
- 687 [50] Velez-Suberbie, M. L., Betts, J. P. J., Walker, K. L., Robinson, C., Zoro, B., and Keshavarz-Moore,  
688 E. (2018). High throughput automated microbial bioreactor system used for clone selection and rapid  
689 scale-down process optimization. *Biotechnology Progress*, 34(1):58–68.
- 690 [51] Venayak, N., Raj, K., and Mahadevan, R. (2019). Impact framework: A python package for writing  
691 data analysis workflows to interpret microbial physiology. *Metabolic Engineering Communications*, 9.
- 692 [52] Venayak, N., von Kamp, A., Klamt, S., and Mahadevan, R. (2018). MoVE identifies metabolic valves  
693 to switch between phenotypic states. *Nature Communications*, 9(1):5332.
- 694 [53] Virtanen, P., Gommers, R., Oliphant, T. E., Haberland, M., Reddy, T., Cournapeau, D., Burovski,  
695 E., Peterson, P., Weckesser, W., Bright, J., van der Walt, S. J., Brett, M., Wilson, J., Millman, K. J.,  
696 Mayorov, N., Nelson, A. R. J., Jones, E., Kern, R., Larson, E., Carey, C. J., Polat, İ., Feng, Y., Moore,  
697 E. W., VanderPlas, J., Laxalde, D., Perktold, J., Cimrman, R., Henriksen, I., Quintero, E. A., Harris,  
698 C. R., Archibald, A. M., Ribeiro, A. H., Pedregosa, F., van Mulbregt, P., and SciPy 1.0 Contributors  
699 (2020). SciPy 1.0: Fundamental Algorithms for Scientific Computing in Python. *Nature Methods*,  
700 17:261–272.

- 701 [54] Wehrs, M., Tanjore, D., Eng, T., Lievense, J., Pray, T. R., and Mukhopadhyay, A. (2019). Engi-  
702 neering robust production microbes for large-scale cultivation. *Trends in Microbiology*, 27(6):524–537.
- 703 [55] Whitehead, E., Rudolf, F., Kaltenbach, H.-M., and Stelling, J. (2018). Automated Planning Enables  
704 Complex Protocols on Liquid-Handling Robots. *ACS Synthetic Biology*, 7(3):922–932.